A Beaded-String Silicon Anode
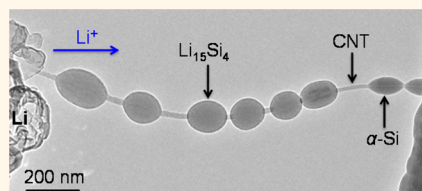
Chuan-Fu Sun,[†,#] Khim Karki,[‡,#] Zheng Jia,[§,#] Hongwei Liao,[†] Yin Zhang,[†,⊥] Teng Li,[§,]* Yue Qi,[¶,]* John Cumings,[‡,]* Gary W. Rubloff,[‡] and YuHuang Wang[†,]*

[†]Department of Chemistry and Biochemistry, [‡]Department of Materials Science and Engineering, and [§]Department of Mechanical Engineering, University of Maryland, College Park, Maryland 20742, United States, [⊥]Department of Physics, Xi'an JiaoTong University, Xi'an, China, and [¶]General Motors Research, 30500 Mound Road, Warren, Michigan 48090, United States. [#]C.-F.S., K.K., and Z.J. contributed equally to this work.

ABSTRACT Interfacial instability is a fundamental issue in heterostructures ranging from biomaterials to joint replacement and electronic packaging. This challenge is particularly intriguing for lithium ion battery anodes comprising silicon as the ion storage material, where ultrahigh capacity is accompanied by vast mechanical stress that threatens delamination of silicon from the current collectors at the other side of the interface. Here, we describe Si-beaded carbon nanotube (CNT) strings whose interface is controlled by chemical functionalization, producing separated amorphous Si beads threaded along mechanically robust and electrically conductive CNT. *In situ* transmission electron microscopy combined with atomic and continuum modeling reveal that the chemically tailored Si—C interface plays important roles in constraining the Si beads, such that they exhibit a symmetric "radial breathing" around the CNT string, remaining crack-free and electrically connected throughout lithiation—delithiation cycling. These findings provide fundamental insights in controlling nanostructured interfaces to effectively respond to demanding environments such as lithium batteries.

KEYWORDS: lithium ion battery · carbon nanotube · nanofabrication · interface · *in situ* TEM · propagation · modeling

Interfacial instability is a fundamental issue in maintaining structural integrality and functionality in heterogeneous materials, especially when different materials respond differently to the thermal, chemical, or electrochemical environmental changes.[1−3] Depending on the balance between adhesive forces and functional driving forces (*e.g.*, differential thermal expansion) that change stress gradients or reactions that modify the materials chemically (*e.g.*, metal silicide formation) or electrochemically (*e.g.*, battery electrode charge/discharge), the interface can become deteriorating and unstable. These issues are particularly challenging for lithium ion battery anodes comprising silicon as the ion storage material. Silicon is a very attractive anode material for lithium ion batteries because it has the highest theoretical capacity, nearly 10 times in excess of conventional graphite electrodes.[4−6] However, the vast mechanical stress that arises from nearly 300% volume changes between lithium insertion and extraction not only causes Si to fracture,[4−6] but also leads to Si delamination from the conductive carbon or copper phases, resulting in quick capacity loss.

Nanostructured Si materials may enable strain relaxation to prevent fracture-induced capacity loss. Spurred by the pioneering work of Chan *et al.*,[7] intensive effort has been recently focused on silicon nanomaterial as a potential anode material for high capacity lithium ion batteries.[8−12] In a one-dimensional silicon nanowire, the mechanical stress that arises during lithiation/delithiation cycles can be effectively relaxed along the radial directions. This reduced-dimension benefit could potentially be maximized in quasi-zero-dimensional nanoparticles, where stress relaxation can occur in all three dimensions. *In situ* TEM studies of the detailed lithiation processes of single Si particles provide direct evidence that silicon nanoparticles below a critical size are indeed immune from cracking.[10]

However, retaining electrical connectivity for silicon nanoparticles in an electrochemically demanding environment remains an even greater challenge to electrode design. Even if nanoparticles do not crack, they easily detach from the current collector or other conducting phases, resulting in undesirable capacity loss.[13,14] To maintain electrical connectivity in Si electrodes, there is substantial interest in incorporating low dimensional carbon nanomaterials such as CNTs and graphene in the design and synthesis of heterostructured Si anodes,[9,15,16] in part because such nanostructures provide
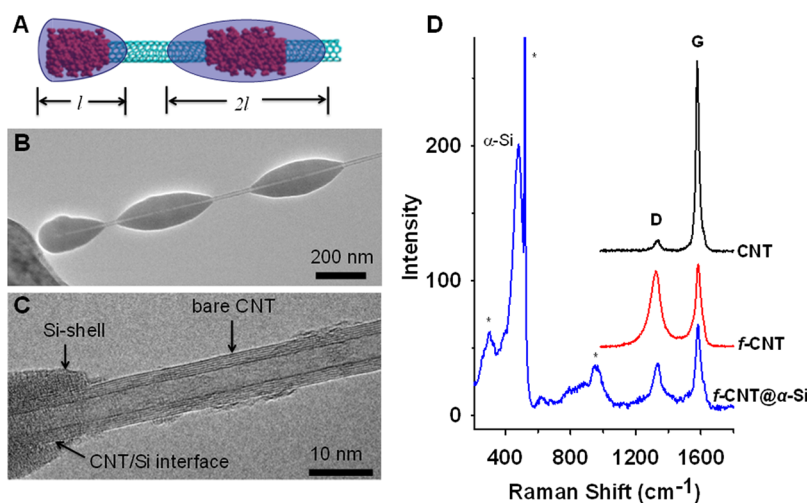
Figure 1. Functional bands control α-Si nucleation on *f*-CNTs. (A) Schematic and (B) TEM images showing symmetrical relation of α-Si beads on the end and sidewall of a *f*-CNT. (C) HRTEM images show the bare CNT between two Si beads and the interface of CNT-core/α-Si-shell. (D) Raman spectra of *f*-CNT@α-Si beaded-string structures in comparison with the pristine CNTs and alkylcarboxylated CNTs. The peaks marked by the asterisk (∗) arise from the crystalline silicon substrate. The excitation line was 632.8 nm.

complementary properties including excellent electrical conductivity and mechanical durability. However, the native adhesion between Si and sp^2 carbon layers has proven to be inherently weak,[15,17] and interfacial delamination remains a significant challenge in such nanocomposite materials. With the potential to alleviate this problem, it has already been shown that binders containing carboxyl groups can enhance stability, thus reducing irreversible capacity loss;[11,18−21] however, the detailed mechanisms are largely unknown.

Here, we demonstrate the synthesis of electrically connected silicon beads on covalently functionalized CNT (*f*-CNT) strings to create a beaded-string structure that does not crack during lithiation−delithiation cycling. Carboxylic functional groups are covalently attached to the sp^2 carbon lattice in a unique "banding" fashion, allowing the growth of discrete amorphous silicon beads symmetrically threaded along the CNT at regular intervals with strong interfacial bonding due to the high density functional groups. This beaded-string structure affords advantageous features unattainable in a conventional continuous coaxial morphology, where Si is uniformly coated on CNTs over the entire surface. Both theoretical modeling and comparative *in situ* TEM studies reveal remarkably improved structural durability of this novel beaded-string structure during lithiation and delithiation.

RESULTS AND DISCUSSION

Controlled Synthesis and Characterization of Beaded-String and Core−Shell Structures. Arc-discharge multiwall carbon nanotubes are chosen for this study because their high crystallinity and low defect-density are ideal for synthesis of well-defined model heterostructures. Functional bands of $-(CH_2)_5COOH$ groups are covalently attached to the outermost walls through C−C

bonds using a propagation chemistry developed previously by some of us.[22] Unlike oxidative chemistries, this propagation chemistry does not remove carbon atoms from the sp^2 lattice of a CNT. Each functional group is instead amplified into a band consisting of hundreds of $-(CH_2)_5COOH$ groups. Amorphous Si (α-Si) is grown on both the *f*-CNTs and on pristine CNTs at 460 °C by low pressure chemical vapor deposition using silane as the silicon source.

We found that the surface chemistry of CNTs plays a vital role in controlling the growth of α-Si on the CNTs. For *f*-CNTs, the functional bands serve as nucleation centers, from which the growth of α-Si starts and extends axially away in both directions, leading to a beaded-string structure with discrete ellipsoidal α-Si beads threaded on the nanotube (Figure 1 and Supporting Information, Figure S1). All α-Si beads have similar axial length, except those at the end of CNTs, which are half-beads. This difference can be explained by assuming that Si can grow in only one direction at the end of a CNT but in both directions from functional bands on the CNT sidewall. All Si beads in an *f*-CNT@α-Si structure have a similar shape and diameter. High resolution transmission electron microscopy (HRTEM) images (Figure 1C and Supporting Information, Figure S3c) clearly show a well-defined *f*-CNT/Si interface, with the segment between two adjacent Si beads being a bare CNT with little Si coating. SEM and TEM images collected at different rotation angles confirm that Si grows with nearly perfect rotational symmetry along the nanotube (Supporting Information, Figure S4). Micro-Raman spectroscopy confirms the characteristic G and G′ peaks of CNT at 1580 and 2660 cm^{-1}, respectively, as well as the peak of α-Si around 480 cm^{-1} (Figure 1D). Covalent attachment of alkylcarboxylic functional groups to the nanotube sidewall introduces sp^3 defect centers,
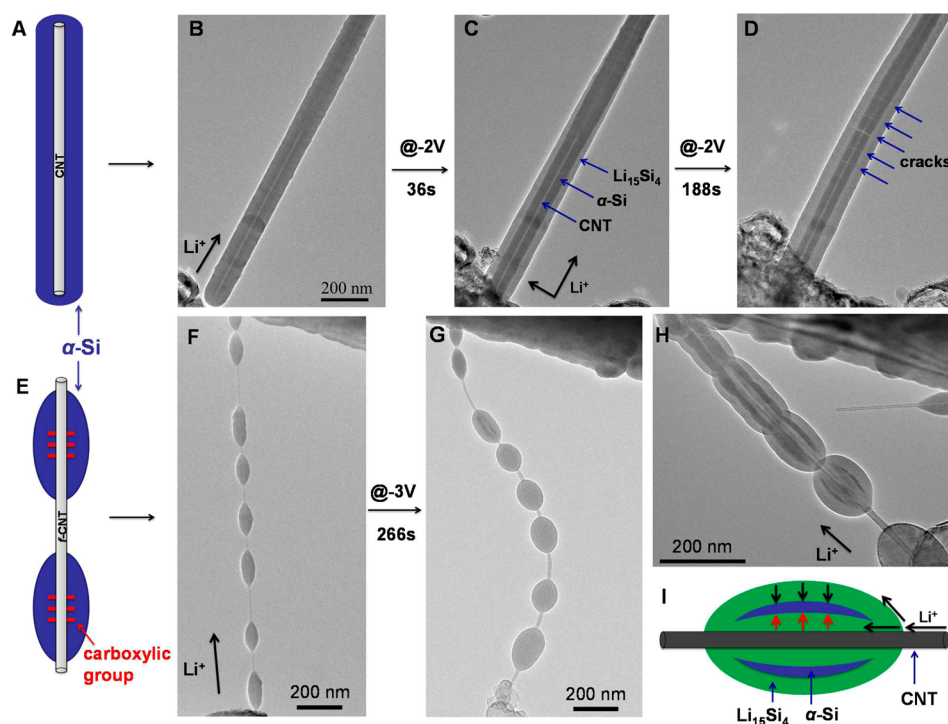
Figure 2. Microstructural evolution of beaded-string heterostructures upon lithiation propagation. (A,E) Schematic drawings show two different nucleation models with the free sliding and fixed interfaces. **(B–D)** Microstructural evolution of CNT@α-Si core–shell structure upon lithiation. **(F,G)** Microstructural evolution of f-CNT@α-Si beaded-string structure upon lithiation. **(H)** Microstructural evolution of f-CNT@α-Si upon lithiation (0 V, t = 15 s) shows that Li$^+$ propagated in two pathways: along both the α-Si surface and CNT/Si interface in the radial direction. **(I)** Schematic drawing indicates two reaction fronts for the formation of Li$_{15}$Si$_4$ in f-CNT@α-Si beaded-string structure.

which activate the disorder mode around 1325 cm^{-1}. This disorder peak persists in the beaded-string structures, suggesting a CNT surface chemistry-dictated CNT/Si interface. In contrast, for pristine, unfunctionalized CNTs, a uniform, continuous α-Si coating is typically formed (Figure 2A,B). This is attributed to uniform nucleation on the nearly defect-free and atomically smooth surface of a pristine CNT.

Electrochemical Evolution of Beaded-String and Core–Shell Si Electrodes. To follow the structural evolution of these heterostructured electrodes, a prototype nanoscale electrochemical cell is built inside the TEM (Supporting Information, Figure S5) using lithium metal as a counter electrode and its native surface Li$_2$O layer as an electrolyte.[12,23] As the Li$_2$O electrolyte is brought into contact with the CNT@α-Si/f-CNT@α-Si heterostructure using an *in situ* nanomanipulator, a constant bias with respect to Li metal (−2 V unless otherwise specified) is applied to the nanowire. Upon application of the electrochemical bias, lithium rapidly propagates axially toward the opposite end of the structure (Supporting Information, movies S1 and S2). The propagation front is evident as a two-phase structure consisting of unreacted silicon (dark) and fully lithiated silicon (light), both being amorphous (Figure 2). Electron diffraction patterns of lithiated beads clearly indicate the formation of the crystalline Li$_{15}$Si$_4$ (c-Li$_{15}$Si$_4$) phase, Li$_2$O, and an amorphous Li$_x$Si (α-Li$_x$Si) alloy at room temperature (Supporting Information, Figure S6),

consistent with previous studies.[12,16] Therefore the dark/light interface in TEM observations represents the c-Li$_{15}$Si$_4$/α-Si interface. The rotational symmetry of the beads is retained in the lithiated structure (Supporting Information, Figure S7), which results from the isotropic propagation of lithiation reaction front in the α-Si beads. Note this lithiation mode of α-Si is in stark contrast with that of crystalline Si, in which anisotropic reaction rate in crystalline Si can lead to faceted or asymmetric nanostructures after lithiation.[12,24]

We found that lithium quickly diffuses along the surface of the α-Si in the axial direction, followed by a lithiation reaction front propagating from the outer surface of α-Si radially inward toward the CNT at the center (Figure 2 and Supporting Information, Figure S8). As a result, a tapered lithiation front is formed in the α-Si during the lithiation process. In the core–shell structures, Li$^+$ propagates along the axial direction at a high rate of 140 ± 10 nm/s, in agreement with previous literature.[16] The propagation along the radial direction is much slower than the lithium diffusion along the axial direction. In contrast, the beaded-string structure has a markedly different morphology change upon lithiation (Figure 2G). Besides the surface reaction, radially inward from the outer surface of each bead, there is also a second lithiation front propagating outward from the CNT/Si interface toward the outer surface (Figure 2H,I). This new reaction pathway is not observed with the
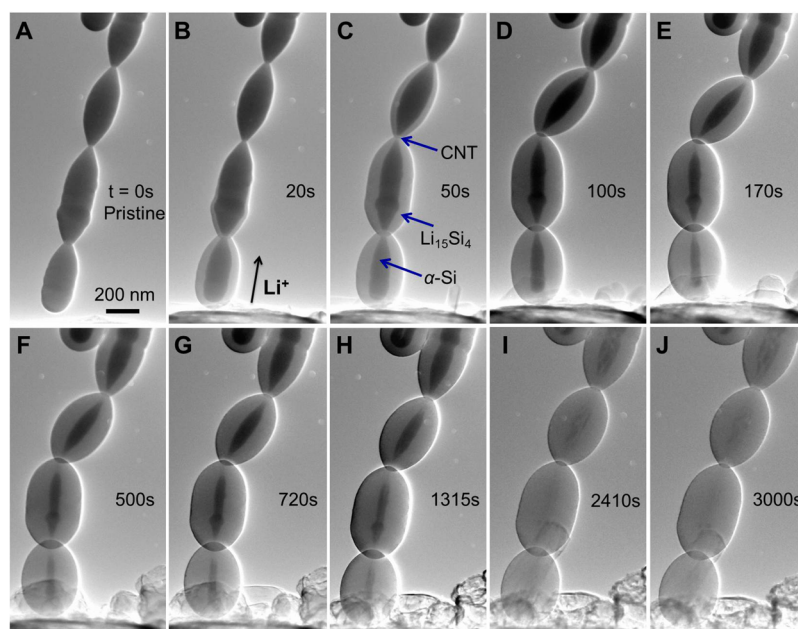
Figure 3. Lithium ions propagate along a string of merging silicon beads. Upon lithiation, the average diameter of the silicon beads increased from 198 nm in the pristine structure (A) to 352 nm in (J). Note the purely radial expansion, which prevents the beads from coalescing, even though they are nearly touching at the beginning.

core–shell structures grown on relatively defect-free CNTs. The two radial reaction front propagating rates, inward and outward, are ~1.7 and ~1 nm/s, respectively (Supporting Information, Figure S9). Both propagation rates are faster than the radial propagation rate in the core–shell structure, which is 0.24–0.9 nm/s. This fast, interfacial propagation pathway, similar to that reported by Wang et al.,[25] can be attributed to the finite length of the beads and the fast diffusion of Li^+ on both Si and CNT surfaces. This results in the beaded-string structure reaching full lithiation faster than the core–shell structure, leading to improved rate capability.

Notably, the beaded-string exhibits remarkable flexibility in accommodating the volume expansion during lithiation. Upon lithiation, the unlithiated portion of the α-Si shell of the continuous core–shell heterostructure tends to crack across the axial direction (Figure 2D, Supporting Information, Figures S8 and S17). Even by slow and gentle lithiation of comparable structures at a minimum bias (0 V) with respect to lithium metal, the α-Si shell failed to avert the formation of these cracks (Supporting Information, Figure S11a). Such fragmentation of the unlithiated Si shell can severely degrade the cycle stability of CNT@α-Si electrodes. By contrast, all f-CNT@α-Si beaded-string electrodes sustained significant lithiation-induced deformation without appreciable fracture, suggesting a highly robust noncracking nanostructure design of anodes for lithium ion batteries.

To further evaluate the stability of beaded-string structures, we followed the lithiation and delithiation of these structures for many cycles with in situ TEM (Supporting Information, Figure S12). Constant biases

of −0.1 V and +3 V with respect to lithium metal are applied to the beaded-string structures during lithiation and delithiation, respectively. The complete state of lithiation and delithiation is assessed by the observable morphological changes in the structures, which stabilize toward the lithiated and delithiated states. During the initial eight cycles, the volume expansion of the lithiated beads nearly reached the theoretical limit. We note that the delithiated silicon did not recover its original size, probably due to the incomplete removal of Li during delithiation or the generation of pores and/or voids, as previously observed in Ge nanowires.[26] However, analysis of the changes in diameter and length of Si beads over 18 cycles reveals a consistent and reliable "radial breathing mode" of expansion and contraction as Li^+ inserts and extracts from the silicon beads (see also Supporting Information, movies S2 and S3). The axial length of the beads barely changes over all cycles, while the main volume expansion is reflected only in the changing radius of the beads. This radial breathing mode further suggests highly reversible mechanical durability of the beaded-string structures.

One major concern with nanoparticle-based electrode materials is their low volumetric storage capacity due to the large inaccessible interparticle space. We found that with beaded-string structures, the silicon beads can be grown during synthesis to the point where adjacent beads just begin to touch and even merge slightly. Since the Si beads do not elongate axially upon lithiation, the spacing between beads can be designed to be very small. An example is shown in Figure 3 where Si beads with diameters approaching 200 nm were grown on a CNT of merely ~20 nm in
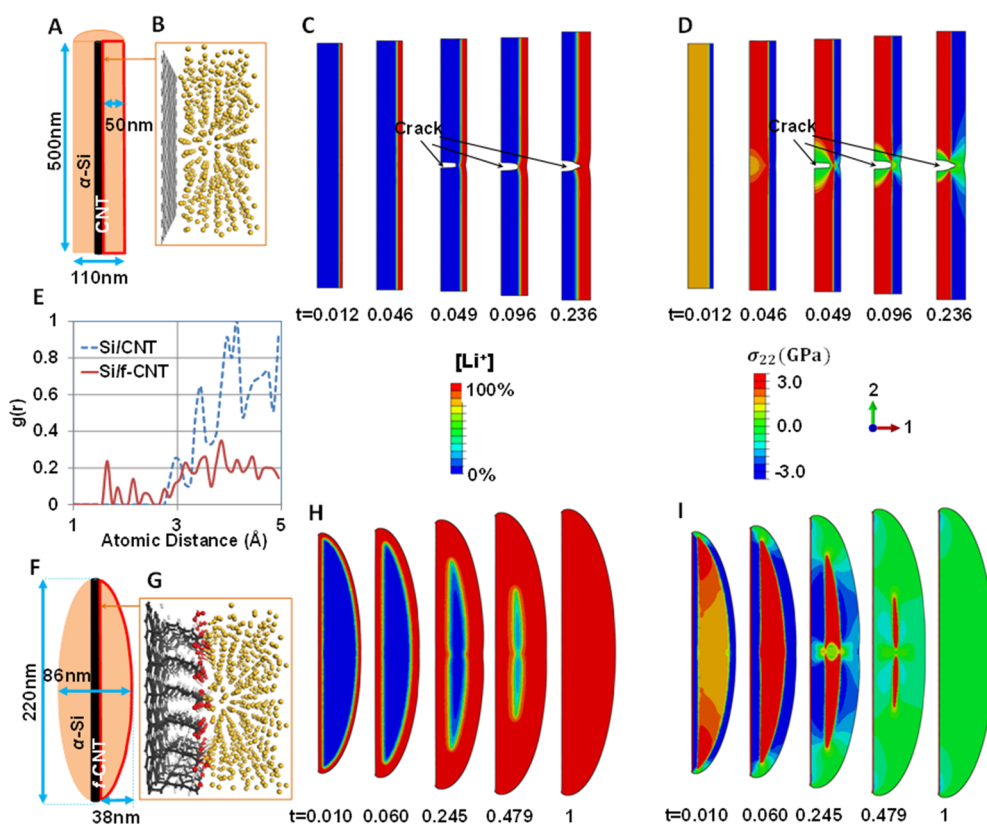
Figure 4. DFT and FEM simulations of the Si–C interface and lithiation-induced stress in Si. (A–D) CNT@α-Si core–shell structure and (F–I), *f*-CNT@α-Si beaded-string structure; (A,F) schematics of the FEM models. Taking advantage of rotational symmetry, only the part demarcated by red solid lines is modeled. (B,G) DFT-minimized atomic structures of the α-Si (gold color) on unmodified graphene surface and −(CH₂)₅COOH-modified graphene surface (C, gray; O, red; H, white), respectively. The $g(r)$ for the atomic pairs across the interface is shown in part E. The bond distance of Si–O, Si–C bonds are in the range of 1.6–2.3 Å. Snapshots of the distribution of normalized Li⁺ concentration (C) and stress component along axial direction (D) in CNT@α-Si core–shell structure at five sequential lithiation stages, respectively: *t* denotes normalized simulation time (=1 for full lithiation). Note the sharp reaction front separating the fully lithiated Si phase and unlithiated Si phase, and the crack initiation and propagation in the unlithiated Si phase due to high axial tensile stress. Parts H and I plot the corresponding snapshots in *f*-CNT@α-Si beaded-string structure at five sequential lithiation stages. Simulations capture the morphology and Li⁺ concentration profile as observed in the experiment. Note that the Si bead can sustain full lithiation without fracture and the overall stress level after full lithiation becomes negligible.

diameter. *In situ* TEM studies confirm noncracking behaviors in all such beaded-string structures investigated. The diameter of these Si beads is ∼33% larger than the critical size (∼150 nm) for nonfracture silicon nanoparticles.[10] Therefore, these beaded-strings can have a volumetric capacity comparable to that of silicon nanowires, but with better cycle life due to their enhanced mechanical durability. We note that in these larger beads, the second interfacial lithiation pathway is lost, probably because all the CNT surfaces are covered by silicon making it behave virtually like a core–shell structure with respect to lithium diffusion. However, the noncracking behavior is again clearly evident.

Theoretical Modeling. We attribute the unique deformation behaviors of beaded-string electrodes to the significantly improved bond strength of the CNT–Si interfaces. To elucidate the atomistic details of this interface, we numerically model a graphene plane consisting of 64 C-atoms, two of which are covalently bonded with −(CH₂)₅COOH functional groups, and Si atoms randomly packed onto the functionalized

graphene surface to approximate an amorphous structure. Density functional theory (DFT) calculations (see Supporting Information for details) reveal that, in the optimized structure, the C=O bond in the −(CH₂)₅COOH group is broken, bonding instead with two Si atoms as −Si–C–O–Si−, covalently connecting the functional group to the amorphous Si. The work of separation, W_{sep}, of the native CNT/Si interface (Figure 4B) in the CNT@α-Si core–shell nanostructure is rather weak, with $W_{sep} \approx 0.10$ J/m² (similar to that computed from DFT for Si on graphite basal plane[17]). We found that covalently attached −(CH₂)₅COOH functional groups, at a 12.5% surface coverage as experimentally estimated,[22] leads to $W_{sep} \approx 0.40$ J/m², four times higher than Si on pristine CNTs. A plot of the radial distribution function $g(r)$ of atomic pairs shows that various chemical bonds, including Si–O and C–Si bonds, are developed at the *f*-CNT/α-CNT interface (the solid line in Figure 4E). Owing to these covalent bonds between the functional group and Si, the interfacial strength in the beaded-string nanostructure is substantially enhanced.

Finite element modeling (FEM) further shows that the difference in interfacial bonding strength leads to the fracture mechanisms of core—shell structures and the crack-avoiding properties of the beaded-string structures (Figure 4). The simulations clearly capture the lithiation process of both structures, as observed in TEM. The lithiation-induced volume expansion leads to compressive stress in the axial direction in the Li^+-rich phase of the α-Si shell, which is balanced by the axial tensile stress in the unlithiated α-Si shell. In the continuous core—shell structure, as the lithiation front sweeps from the outer surface into the α-Si shell, the axial tensile stress in the unlithiated α-Si shell increases monotonically. Because of poor bonding between the Si and the CNT core, there is effectively no load transfer to the high strength sp^2 carbon, leaving a free inner surface for the Si shell.[15] Once the axial tensile stress exceeds the cohesion strength of α-Si, cracks initiate from the free inner surface of the α-Si shell and propagate along the radial direction outward (Figure 4D). This radial crack propagation is arrested near the reaction front due to the compressive stress in the fully lithiated phase, agreeing well with experimental observations. For the f-CNT@α-Si beaded-string structure, even though the unlithiated phase of the α-Si bead is under tension, the magnitude of the tensile stress is effectively mitigated due to the strong mechanical constraint of the chemically tailored Si—C interface (Figure 4I). As a result, the axial tensile stress in the α-Si bead is never high enough to initiate cracks in the unlithiated Si. Without the strong mechanical constraint of the f-CNT, Li^+ diffusion along the α-Si bead inner surface can only help mitigate the axial tensile stress in the unlithiated phase but cannot sufficiently avert its cracking (Supporting Information, Figures S13 and S14). By contrast, if the f-CNT/α-Si interface is strong enough, the α-Si bead can survive full lithiation without cracking, even if Li^+ diffusion only occurs from the bead outer surface (Supporting Information, Figure S15), as experimentally observed in merging beads.

CONCLUSIONS

f-CNT@α-Si beaded-string heterostructures with chemically tailored carbon—silicon interfaces were designed and synthesized based on a fundamental understanding of carbon surface chemistry and Si nucleation on covalently modified CNT surfaces. In situ TEM studies of lithiation propagation reveal that these novel heterostructures can accommodate huge volume changes during lithiation and delithiation without appreciable mechanical failure. By contrast, CNT@α-Si continuous core—shell nanostructures fracture upon lithiation. DFT and continuum FEM studies consistently suggest that the strong Si—C interface made possible by the carboxylic functional bands on CNTs plays key roles in enabling noncracking f-CNT@α-Si beaded-string heterostructures. These findings thus provide important new insights in the synthesis of high performance Si electrodes, laying a foundation for next-generation lithium ion batteries.

METHODS

Controlled Synthesis of CNT@α-Si/f-CNT@α-Si Heterostructures. Crystalline arc-discharge multiwall CNTs, with few surface defects and a diameter range of 2—50 nm, were covalently functionalized with —$(CH_2)_5COOH$ groups using a propagation chemistry as described previously.[22] The functionalized CNTs were dispersed in aqueous sodium hydroxide solution (pH = 10) and then extracted with hexane to separate the less functionalized CNTs into a hexane layer, leaving the f-CNTs in water. The large and small graphitic particles that typically contaminate arc discharge CNTs were removed by centrifugation at 3000 and 16000 rpm, respectively. Then, the purified f-CNTs solution was drop-cast onto a clean Si(100) thin-wafer substrate (250 μm). After drying in air and rinsing with ultrapure deionized water three times to remove salts, the Si substrate was cleaved, leaving a controllable number of cantilevered f-CNTs protruding over the cleaved edge. Nonfunctionalized arc-discharge CNTs were used as control. Amorphous Si was grown on the f-CNTs and CNTs at 460 °C in a low pressure chemical vapor deposition (LPCVD) system (Atomate Nanowire Growth System) using 2 Torr of silane as the silicon source and 1 Torr of argon as the protective gas. The thickness of the amorphous Si shell was controlled by the growth time.

Structural Characterization and in Situ TEM Studies. Raman scattering spectra were collected on a Horiba Yvon LabRam ARAMIS Raman spectroscope with a helium neon laser excitation source (632.8 nm). Scanning electron microscopy (SEM) images were collected using a SU-70 SEM (Hitachi) at 3 or 10 kV with an emission current of 33 μA. In situ characterization was employed using a JEOL JEM-2100 LaB$_6$ TEM operating at 200 kV. We use a specialized piezoactuated Nanofactory holder which simultaneously allows manipulation and imaging with three degrees of freedom in real-time. Lithiation and delithiation were controlled by applying constant voltages ranging from -3 to 0 V and $+1$ to $+3$ V, respectively. The manipulation tip carries a piece of lithium metal, which acts as a Li source and a counter electrode. The thin native Li_2O layer, which is formed on the surface of pristine Li metal inside the TEM due to residual O_2 and H_2O gas in the TEM column, serves as a solid-state electrolyte, allowing the diffusion of Li^+ between the electrodes under potential bias.[23,27]

DFT Calculations. All first-principles calculations were conducted with the Vienna ab Initio Simulation Package (VASP), a plane wave density functional code.[28] Potentials constructed by the projector-augmented wave (PAW) method[29] were used for the elements. The exchange-correlation part of the density functional was treated within the local density approximation (LDA) of Ceperley-Alder[30] as parametrized by Perdew and Zunger.[31] From convergence studies, we determined the kinetic energy cutoff in the plane wave expansion to be 400 eV and a $3 \times 3 \times 1$ Monkhorst-Pack k-mesh[32] for the slab modeled. The amorphous Si was generated via ab intio molecular dynamics simulation and used in previous elastic properties calculations for lithiated silicon.[33] All the relaxed structures achieved a Hellman-Feynman force convergence of 0.05 eV/Å. To determine the energy required to break the interfacial bonds on a unit area, W_{sep}, we constructed a flat single sheet of graphene with and without surface modifications. This is reasonable considering the diameter of the CNT used in the experiment is larger than 10 nm. Thus the W_{sep} for the slab interface model is defined as

$$W_{sep} = \frac{1}{A}[E_{Si} + E_{sub} - E_{interface}]$$

where E_{Si}, E_{sub}, and $E_{interface}$ are the total energies of the relaxed atomic structures of amorphous Si, substrate (graphene or modified graphene), and the interface of the two phases, respectively. The radial distribution $g(r)$ is computed only for atomic pairs between the Si phase and the substrate in the interface structure.

Finite Element Modeling. To model the evolving lithiatiated/pristine Si interface, we adopt an isotropic diffusivity of Li^+ in Si with a nonlinear dependence on Li^+ concentration in our model. The diffusion-induced stress is simultaneously calculated through a coupled chemomechanical model as the distribution of Li^+ concentration evolves. We implement cohesive zone elements at locations that are most susceptible to cracking (see Supporting Information for details of FEM simulations). For the CNT@α-Si core−shell nanostructure, the inner surface of the α-Si shell is set to be free, as suggested by the rather weak interface with the CNT. Li^+ can diffuse into the α-Si shell only from its outer surface, as shown in the experiments. For the f-CNT@α-Si beaded-string nanostructure, the inner surface of the α-Si shell is covalently bonded to a CNT, giving the strong interface between α-Si and the functionalized CNT surface.

Conflict of Interest: The authors declare no competing financial interest.

REFERENCES AND NOTES

1. Fratzl, P.; Weinkamer, R. Nature's Hierarchical Materials. *Prog. Mater. Sci.* **2007**, *52*, 1263–1334.
2. Ho, P. S.; Hahn, P. O.; Bartha, J. W.; Rubloff, G. W.; LeGoues, F. K.; Silverman, B. D. Chemical Bonding and Reaction at Metal/Polymer Interfaces. *J. Vac. Sci. Technol., A* **1985**, *3*, 739–745.
3. Lucksanasomboool, P.; Higgs, W. A. J.; Higgs, R. J. E. D.; Swain, M. V. Interfacial Fracture Toughness between Bovine Cortical Bone and Cements. *Biomater* **2003**, *24*, 1159–1166.
4. Sharma, R. A. Thermodynamic Properties of the Lithium−Silicon System. *J. Electrochem. Soc.* **1976**, *123*, 1763–1768.
5. Boukamp, B. A.; Lesh, G. C.; Huggins, R. A. All-Solid Lithium Electrodes with Mixed-Conductor Matrix. *J. Electrochem. Soc.* **1981**, *128*, 725–729.
6. Obrovac, M. N.; Christensen, L. Structural Changes in Silicon Anodes During Lithium Insertion/Extraction. *Electrochem. Solid-State Lett* **2004**, *7*, A93–A96.
7. Chan, C. K.; Peng, H. L.; Liu, G.; McIlwrath, K.; Zhang, X. F.; Huggins, R. A.; Cui, Y. High-Performance Lithium Battery Anodes Using Silicon Nanowires. *Nat. Nanotechnol.* **2008**, *3*, 31–35.
8. Wu, H.; Chan, G.; Choi, J. W.; Ryu, I.; Yao, Y.; McDowell, M. T.; Lee, S. W.; Jackson, A.; Yang, Y.; Hu, L.; et al. Stable Cycling of Double-Walled Silicon Nanotube Battery Anodes Through Solid-Electrolyte Interphase Control. *Nat. Nanotechnol.* **2012**, *7*, 309–314.
9. Hu, L. B.; Wu, H.; Gao, Y. F.; Cao, A. Y.; Li, H. B.; McDough, J.; Xie, X.; Zhou, M.; Cui, Y. Silicon−Carbon Nanotube Coaxial Sponge as Li-Ion Anodes with High Areal Capacity. *Adv. Energy Mater* **2011**, *1*, 523–527.
10. Liu, X. H.; Zhong, L.; Huang, S.; Mao, S. X.; Zhu, T.; Huang, J. Y. Size-Dependent Fracture of Silicon Nanoparticles during Lithiation. *ACS Nano* **2012**, *6*, 1522–1531.
11. Bridel, J. S.; Azais, T.; Morcrette, M.; Tarascon, J. M.; Larcher, D. Key Parameters Governing the Reversibility of Si/Carbon/CMC Electrodes for Li-Ion Batteries. *Chem. Mater.* **2010**, *22*, 1229–1241.
12. Liu, X. H.; Zheng, H.; Zhong, L.; Huan, S.; Karki, K.; Zhang, L. Q.; Liu, Y.; Kushima, A.; Liang, W. T.; Wang, J. W.; et al. Anisotropic Swelling and Fracture of Silicon Nanowires during Lithiation. *Nano Lett.* **2011**, *11*, 3312–3318.
13. Chen, Z. H.; Christensen, L.; Dahn, J. R. A Study of the Mechanical and Electrical Properties of a Polymer/Carbon Black Binder System Used in Battery Electrodes. *J. Appl. Polym. Sci.* **2003**, *90*, 1891–1899.
14. Christensen, J. Modeling Diffusion-Induced Stress in Li-Ion Cells with Porous Electrodes. *J. Electrochem. Soc.* **2010**, *157*, A366–A380.
15. Liao, H.; Karki, K.; Zhang, Y.; Cumings, J.; Wang, Y. Interfacial Mechanics of Carbon Nanotube@Amorphous-Si Coaxial Nanostructures. *Adv. Mater.* **2011**, *23*, 4318–4322.
16. Wang, C. M.; Li, X.; Wang, Z.; Xu, W.; Liu, J.; Gao, F.; Kovarik, L.; Zhang, J.-G.; Howe, J.; Burton, D. J.; et al. In Situ TEM Investigation of Congruent Phase Transition and Structural Evolution of Nanostructured Silicon/Carbon Anode for Lithium Ion Batteries. *Nano Lett.* **2012**, *12*, 1624–1632.
17. Howe, J. Y.; Burton, D. J.; Qi, Y.; Meyer Iii, H. M.; Nazri, M.; Nazri, G. A.; Palmer, A. C.; Lake, P. D. Improving Microstructure of Silicon/Carbon Nanofiber Composites as a Li Battery Anode. *J. Power Sources* **2013**, *221*, 455–461.
18. Fransson, L.; Eriksson, T.; Edstrom, K.; Gustafsson, T.; Thomas, J. O. Influence of Carbon Black and Binder on Li-Ion Batteries. *J. Power Sources* **2001**, *101*, 1–9.
19. Zhang, S. S.; Jow, T. R. Study of Poly(acrylonitrile-methyl methacrylate) as Binder for Graphite Anode and $LiMn_2O_4$ Cathode of Li-Ion Batteries. *J. Power Sources* **2002**, *109*, 422–426.
20. Guy, D.; Lestriez, B.; Guyomard, D. New Composite Electrode Architecture and Improved Battery Performance from the Smart Use of Polymers and Their Properties. *Adv. Mater.* **2004**, *16*, 553–557.
21. Kovalenko, I.; Zdyrko, B.; Magasinski, A.; Hertzberg, B.; Milicev, Z.; Burtovyy, R.; Luzinov, I.; Yushin, G. A Major Constituent of Brown Algae for Use in High-Capacity Li-Ion Batteries. *Science* **2011**, *333*, 75–79.
22. Deng, S.; Zhang, Y.; Brozena, A. H.; Mayes, M. L.; Banerjee, P.; Chiou, W.-A.; Rubloff, G. W.; Schatz, G. C.; Wang, Y. Confined Propagation of Covalent Chemical Reactions on Single-Walled Carbon Nanotubes. *Nat. Commun.* **2011**, *2*, article no. 382, DOI: 10.1038/ncomms1384.
23. Karki, K.; Epstein, E.; Cho, J.-H.; Jia, Z.; Li, T.; Picraux, S. T.; Wang, C.; Cumings, J. Lithium-Assisted Electrochemical Welding in Silicon Nanowire Battery Electrodes. *Nano Lett.* **2012**, *12*, 1392–1397.
24. Goldman, J. L.; Long, B. R.; Gewirth, A. A.; Nuzzo, R. G. Strain Anisotropies and Self-Limiting Capacities in Single-Crystalline 3D Silicon Microstructures: Models for High Energy Density Lithium-Ion Battery Anodes. *Adv. Funct. Mater.* **2011**, *21*, 2412–2422.
25. Wang, W. W.; Liu, X. H.; Zhao, K.; Palmer, A.; Patten, E.; Burton, D.; Mao, X. M.; Suo, Z.; Huang, J. Y. Sandwich-Lithiation and Longitudinal Crack in Amorphous Silicon Coated on Carbon Nanofibers. *ACS Nano* **2012**, *6*, 9158–9167.
26. Liu, X. H.; Huang, S.; Picraux, S. T.; Li, J.; Zhu, T.; Huang, J. Y. Reversible Nanopore Formation in Ge Nanowires during Lithiation−Delithiation Cycling: an *in Situ* Transmission Electron Microscopy Study. *Nano Lett.* **2011**, *11*, 3991–3997.
27. Liu, X. H.; Zhang, L. Q.; Zhong, L.; Liu, Y.; Zheng, H.; Wang, J. W.; Cho, J.-H.; Dayeh, S. A.; Picraux, S. T.; Sullivan, J. P.; et al. Ultrafast Electrochemical Lithiation of Individual Si Nanowire Anodes. *Nano Lett.* **2011**, *11*, 2251–2258.
28. Kresse, G.; Furthmuller, J. Efficient Iterative Schemes for *ab Initio* Total-Energy Calculations using a Plane-Wave Basis Set. *Phys. Rev. B* **1996**, *54*, 11169–11186.

29. Blöchl, P. E. Projector Augmented-Wave Method. *Phys. Rev. B* **1994**, *50*, 17953–17979.
30. Ceperley, D. M.; Alder, B. J. Ground State of the Electron Gas by a Stochastic Method. *Phys. Rev. Lett.* **1980**, *45*, 566–569.
31. Perdew, J. P.; Zunger, A. Self-Interaction Correction to Density-Functional Approximations for Many-Electron Systems. *Phys. Rev. B* **1981**, *23*, 5048–5079.
32. Monkhorst, H. J.; Pack, J. D. Special Points for Brillouin-Zone Integrations. *Phys. Rev. B* **1976**, *13*, 5188–5192.
33. Shenoy, V. B.; Johari, P.; Qi, Y. Elastic Softening of Amorphous and Crystalline Li—Si Phases with Increasing Li Concentration: A First-Principles Study. *J. Power Sources* **2010**, *195*, 6825–6830.